JACS
JOURNAL OF THE AMERICAN CHEMICAL SOCIETY

Communication

pubs.acs.org/JACS

Giant Raman Response to the Encapsulation of Sulfur in Narrow Diameter Single-Walled Carbon Nanotubes

Guanghui Li,[†,§] Chengyin Fu,[†] M. Belén Oviedo,[†] Mingguang Chen,[†,§] Xiaojuan Tian,[†,§] Elena Bekyarova,[‡,§] Mikhail E. Itkis,[‡,§] Bryan M. Wong,[†] Juchen Guo,[†] and Robert C. Haddon*[,†,‡,§]

[†]Department of Chemical Engineering, [‡]Department of Chemistry, and [§]Center for Nanoscale Science and Engineering, University of California, Riverside, California 92521, United States

Supporting Information

ABSTRACT: Encapsulation of sulfur in HiPCO-SWNTs leads to large changes in the Raman spectra with the appearance of new peaks at 319, 395, and 715 cm^{-1} which originate from the sulfur species within the SWNTs, while the high frequency SWNT bands (ν > 1200 cm^{-1}) are decreased in intensity. The encapsulated species also shifts the near-IR interband electronic transitions to lower energy by more than 10%. These effects seem to originate with the van der Waals interaction of the confined sulfur species with the walls of the SWNTs which are not expected to be significant in the case of the previously studied large diameter SWNTs. We suggest that sulfur in the small diameter SWNTs exists as a helical polymeric sulfur chain that enters the SWNT interior in the form of S_2 ($^3\Sigma_g^-$) molecules which undergo polymerization to linear diradicals.

Lithium-sulfur batteries are of current interest because of the high capacity of sulfur as a cathode for rechargeable batteries when paired with metallic elements such as lithium. The use of carbon-based materials, including single-walled carbon nanotubes (SWNTs), to encapsulate sulfur provides an interesting approach to the study of the electrochemical lithiation process at the cathode in which there is confinement of the active sulfur species.[1−6] Apart from the electrochemical experiments, these materials have been studied by X-ray diffraction, Raman spectroscopy, XPS, TGA, and theoretical calculations.[7,8] The results of these studies have been interpreted in terms of metallic, linear one-dimensional chains of sulfur confined within the SWNTs. As far as we could ascertain the previous studies made use of electric arc (EA) produced materials which are known to lead to SWNTs of relatively large diameter (D_{av} ≈ 1.55 nm),[9−11] and the response of the Raman spectra to the presence of encapsulated sulfur is relatively modest as shown in prior reports and in our own experiments (SI). However, when we employed HiPCO-SWNTs in an essentially identical set of sulfur encapsulation experiments, we observed an extremely large modulation of the Raman peak intensities.

Here we report our studies and interpretation of the effect of sulfur encapsulation on the spectroscopic properties of EA- and HiPCO-SWNTs of average diameter, D_{av} = 1.55 ± 0.1 and 1.0 ± 0.2 nm, respectively.[9−11] Our initial studies were focused on the use of these materials in batteries, but in order to unambiguously characterize the effect of sulfur incorporation on the HiPCO-SWNTs, we prepared samples as thin films (thickness, t = 50 nm), by filtration of dispersions.[12] In a typical experiment, HiPCO-SWNTs (Nanointegris, 2 mg) were dispersed in 100 mL of an aqueous solution of sodium cholate (1g) by sonication (5 h). The dispersion was centrifuged at 8000 rpm (11,000 g) for 15 min and then filtered through a cellulose membrane (pore size 50 nm). The resulting SWNT films were transferred to quartz substrates for spectroscopic characterization and sulfur treatment. The sulfur was encapsulated inside the SWNTs by exposure of the thin-film samples to vapor phase sulfur at 600 °C under a static vacuum.

In agreement with previous work, the response of EA-SWNTs to the encapsulation of sulfur (denoted as S@EA-SWNTs) is quite weak (Figure S1).[5,6] There is a discernible effect on the radial breathing mode (RBM) which appears at 150−200 cm^{-1} and an enhancement of peaks centered at 375 cm^{-1},[6] which may correspond to a peak that was previously observed at 390 cm^{-1} in a similar sample.

The response of the HiPCO-SWNTs to the encapsulation of sulfur is much more pronounced (Figures 1 and S2), and prominent peaks appear at 319 and 395 cm^{-1} together with a series of peaks at ∼715 cm^{-1}.

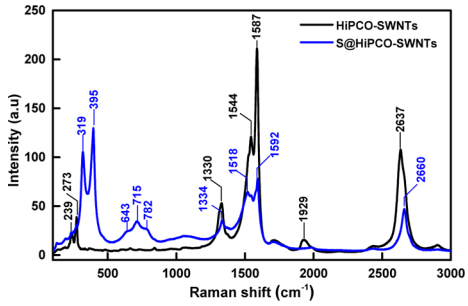

Figure 1. Raman spectra of HiPCO-SWNTs and S@HiPCO-SWNTs films at laser excitation wavelength 532 nm.

We find that these new features disappear when the SWNTs are annealed at high temperatures (Figure S3), and in the case of HiPCO-SWNTs, the sulfur removal process is complete after annealing at 650 °C for 10 h under argon; furthermore we do not find any obvious effect on pristine SWNTs that have been annealed at these temperatures (Figure S4).

Received: October 9, 2015
Published: December 16, 2015

DOI: 10.1021/jacs.5b10598
J. Am. Chem. Soc. 2016, 138, 40−43

The intensities of Raman features are affected by changes in the electronic structure of the carbon nanotubes as well as to perturbations to the restoring forces of the vibrational modes.[13] Thus, in order to provide direct information on the effect of sulfur incorporation on the electronic structure of the SWNTs, we examined the near-infrared and visible (NIR/vis) spectra of the samples, and the results are shown in Figure 2. It is quite clear

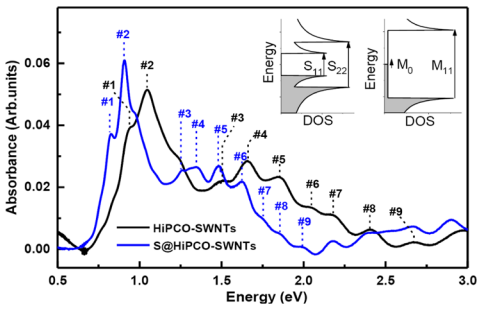

Figure 2. Base-line subtracted near NIR/vis absorption spectra of HiPCO-SWNTs and S@HiPCO-SWNTs films in the vicinity of the S_{11}, S_{22}, and M_{11} interband electronic transitions. Inset: Schematic energy band diagram for semiconducting and metallic SWNTs.

that the features, due to the SWNT interband electronic transitions in the S_{11}, S_{22} (semiconducting) and M_{11} (metallic) regions, are strongly affected in the S@HiPCO-SWNTs, while there is little change in the NIR/vis spectrum of S@EA-SWNTs (Figure S5).

The baseline subtracted NIR/vis spectra are shown in Figure 2, and our best estimates for the assignments are given in Table S1 (nomenclature is shown in inset to Figure 2; note that peak 7 can be assigned to the S_{22} or the M_{11} set of transitions). Thus, the percentage decreases in the NIR/vis transitions due to sulfur encapsulation are $\Delta S_{11} = -13\%$ (1), −13 (2); $\Delta S_{22} = -16$ (3), −18 (4), −20 (5), −20(6), −20 (7); $\Delta M_{11} = -20$ (7), −23 (8), −26 (9). The assignments are based on previous studies of individual HiPCO-SWNTs using absorption and fluorescence spectroscopy,[14−16] and there is a clear trend toward larger shifts in the interband transitions as the band gap energies increase, which is reflected in the percentage decrease in the band gaps among the transitions. There are a number of distinct effects which could be responsible for the shifts in the interband electronic transition energies, and we discuss some of the more likely scenarios below. We begin by emphasizing that the shifts in the band gap energies as result of sulfur encapsulation scale roughly with the energy gaps and thus could be accounted for by an increase in the SWNT diameters or a weakening of the resonance or transfer integral (β). The C−C bonds as the simple tight-binding form of the interband transition energies is given by $S_{11} = 2a\beta/d$, $S_{22} = 4a\beta/d$, and $M_{22} = 6a\beta/d$, where a is the carbon−carbon bond length (nm) and d is the SWNT diameter (nm).[13] If we scale the percentage decreases in the observed interband transition energies by the ratios of the numerical prefactors from the tight binding calculation, we obtain $\Delta S_{11} = -13\%$ (1), −13 (2); $\Delta S_{22}/2 = -8$ (3), −9 (4), −10 (5), −10(6), −10(7); $\Delta M_{11}/3 = -7$ (7), −8 (8), −9 (9). Thus, based on the interband electronic transitions, sulfur encapsulation has a large effect on the electronic structure of the SWNTs, and if this were to be attributed to a change in geometry, it would imply an increase in the SWNT diameters by ∼10%, which is not supported by our calculations (Table S1).

Given the intimate contact between the sulfur chain and the walls of the HiPCO-SWNTs, it is natural to consider the formation of excimers or exciplexes between the two materials,[17] but the nature of the necessary charge-transfer complex does not seem very plausible. Rehybridization effects are known to be important in small diameter SWNTs and probably play a role in the phenomena reported herein.[9,18,19] An important manifestation of this effect is polygonization[20] in which the walls of the SWNTs undergo the type of faceting which is well-known in fullerenes.[21] Polygonization of the SWNT walls is inevitable given the four-fold axial profile of the S_x chain found in our calculations (Figure 4). As in the fullerenes, this distortion serves to concentrate the pyramidalization at certain carbon atoms that become strongly rehybridized.[21,22]

There have been a number of studies of the effect of strain and external pressure on SWNTs that throw light on the origins of the shifts that we observe (Figure 2). Matrix-imposed stress on SWNTs has been shown to produce a chirality-dependent shift of the photoluminescence spectra that divides the samples into two groups depending on their helicity: the first group of SWNTs shows an increase in the energy of the S_{11} transitions and a decrease in the S_{22} energies on cooling frozen dispersions, whereas the second group of SWNTs shows exactly the opposite behavior.[23] These results are in full accord with calculations of the effect of stress along the axis of the SWNTs,[24,25] and thus it appears that the frozen matrix generates uniaxial compressive stress along the SWNTs.

A study of the effect of hydrostatic pressure on the interband transition energies of debundled HiPCO-SWNT suspensions in diamond anvil cells found that the band gap energies moved to lower energies, although the second set of interband transitions (S_{22} in this paper) were much less sensitive to pressure.[19] The authors were unable to fully rationalize these results in terms of previous studies, although they noted the likely importance of the rehybridization of the SWNT electronic structure. Our results are not consistent with either of these previous reports on strain, as we find that all of the electronic transitions move to lower energies with the greatest shifts associated with the higher excitation levels.

The spectral intensity of the Raman features of SWNT samples is strongly enhanced when the experimental laser light is resonant with an interband (excitonic) transition in individual carbon nanotubes.[13,26] As a result, variations in the Raman intensity are usually ascribed to a change in the resonance condition, and there are a number of reports in the literature on the observation of such effects in doped samples.[27−32] In virtually all these cases the Raman intensities are reduced; the only mention we could find of strongly increased intensities in Raman spectra was a report on individual, pristine, suspended quasi-metallic SWNTs in which it was found that all of the transitions are strongly modulated by electrostatic gating due to the proximity of a Mott insulator transition.[33]

The resonant Raman intensity in the Stokes process is given by

$$I^{\mu}(E_{\mathrm{L}}) = C\left|\int \frac{\mathbf{M}^{\mathrm{oa}}\mathbf{M}^{\mathrm{ep}}\mathbf{M}^{\mathrm{oe}}dk}{E_{\mathrm{R}}[E_{\mathrm{R}} - E_{\mathrm{ph}}]}\right|^2 \quad (1)$$

where C is a constant, $E_{\mathrm{R}} = E_{\mathrm{L}} - E_{\mu} - i\gamma$ is the resonance condition, E_{L} is the laser energy (2.41 eV), E_{μ} is the exciton transition energy for the μth set of subbands, E_{ph} is the phonon energy, γ is the resonance broadening energy, $\mathbf{M}^{\mathrm{oa}}$ is the matrix element for the optical absorption process, $\mathbf{M}^{\mathrm{ep}}$ is the electron−phonon coupling matrix element, and $\mathbf{M}^{\mathrm{oe}}$ is the matrix element

DOI: 10.1021/jacs.5b10598
J. Am. Chem. Soc. 2016, 138, 40−43

for the optical emission process.[33−37] As noted above, a likely cause of the drastic modification to the Raman spectra of HiPCO-SWNTs on sulfur encapsulation is a change in the resonance condition (E_R), and this scenario is supported by both the NIR/vis spectroscopy and the DFT calculations carried out on the S@HiPCO-SWNTs (below). The resonance term includes both the interband transition energy (E_μ) and the resonance broadening energy (γ), and it is clear from Figure 2 that both of these quantities are affected by the incorporation of sulfur into HiPCO-SWNTs. The resonance broadening energy is very small in individual SWNTs (γ = 8 meV for a SWNT on Si/SiO_2),[35] but this term is quite sensitive to the nanotube environment and values of γ = 60 meV (SDS wrapped SWNTs) and γ = 120 meV (SWNT bundles) have been reported for HiPCO-SWNTs,[36] and thus it is to be expected that the incorporation of the S_x-helix would further increase the value of γ in the S@HiPCO-SWNTs. As discussed above, the strain induced by the incorporation of sulfur into the HiPCO-SWNTs affects the interband transition energies [E_μ (S_{11}, S_{22}, and M_{11}, above)] and may also be expected to modify the electron−phonon coupling term ($\mathbf{M}^{ep}$). A quantitative assessment of the relative weights of these contributions to the very large changes observed in the Raman spectra of S@HiPCO-SWNTs is beyond the scope of this paper, but we report additional experiments below.

Most of the HiPCO-SWNT Raman intensities are decreased by the incorporation of sulfur in agreement with previous work on perturbed SWNTs,[27,30,31,37] and it is only in the region from 300 to 800 cm^{-1} that new, very strong peaks appear; given the proximity of this region to sulfur−sulfur vibrations in the Raman spectra of the various molecular and polymeric sulfur species, it is natural to consider electron−phonon coupling between the excited states of the SWNTs and the phonons of the sulfur species that are encapsulated. In this way molecular vibrations of the sulfur species could be enhanced in the Raman spectra by the excitonic absorptions of the SWNTs, and we note that the band at 715 cm^{-1} observed in the S@HiPCO-SWNTs is quite close to the value of 716 cm^{-1} observed for S_2 ($^3\Sigma_g^-$) in an argon matrix.[38] Polymeric sulfur (S_x) has bands at ∼460 and ∼425 cm^{-1}[39] which do not correspond to the bands at 395 and 319 cm^{-1} observed in our spectra, although the distortions of the sulfur chains discussed below would likely weaken the stretching frequencies of the vibrations of the S_x@HiPCO-SWNTs, and thus these features could possibly originate from encapsulated sulfur species. Therefore, we carried out encapsulation experiments in which $^{34}S_8$ was used as the source for infusion of sulfur into the HiPCO-SWNTs. Based on prior work in the literature, the isotopic shift in such species is known to closely follow the simple spring constant relationship which gives $\nu_1(^{34}S)/\nu_1(^{32}S) = (32/34)^{1/2} = 0.970$.[39] As we show in Figure 3 and Table S2, the new peaks in the Raman spectra of S@HiPCO-SWNTs exhibit the expected shift for isotopic substitution in species possessing S−S bonds, and this shows unequivocally that the new Raman vibrations originate from encapsulated sulfur species which obtain intensity from electron−phonon coupling to the resonant SWNT excited states.

We carried out DFT calculations on the S@SWNTs (SI) and it is clear that there is ample space inside the EA-SWNTs to accommodate sulfur in the form of S_8 molecules or in polymeric form but this is not the case for the HiPCO-SWNTs which have a much smaller diameter. The most compact form for sulfur encapsulated in SWNTs was found to be a helix with a screw order of four atoms as shown in Figure 4.

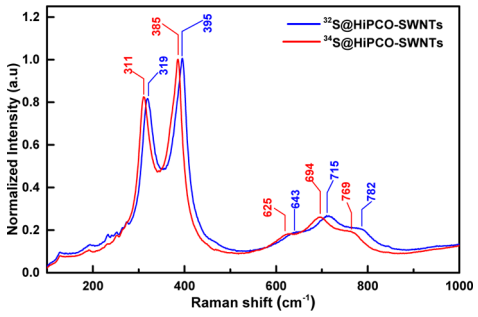

Figure 3. Raman spectra of ^{32}S@HiPCO-SWNTs and ^{34}S@HiPCO-SWNTs films.

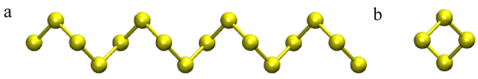

Figure 4. Calculated structure for the sulfur helix in S@SWNTs: (a) side and (b) cross-sectional views.

When this structure was encapsulated in an (11,11) EA-SWNT of diameter 1.6 nm, the preferred diameter of the helix was found to be ∼0.33 nm which gives a van der Waals diameter of ∼0.7 nm (Figure S7). This is easily accommodated in the (11,11) SWNT which has an internal van der Waals diameter of 1.26 nm, but for HiPCO-SWNTs the corresponding typical chirality might be that of a (7,7) SWNT which has a calculated diameter of 0.95 nm and internal van der Waals diameter of ∼0.61 nm (Figure S8). Thus, we anticipate a nonbonded interaction between the sidewalls of HiPCO-SWNTs that is not present in EA-SWNTs, and it may be seen that the preferred helical S_x structure is expected to break the quasi-rotational symmetry of the HiPCO-SWNTs by imposing a four-fold distortion of the sidewalls.

Finally we turn to a consideration of the mechanism for incorporation of sulfur into the SWNTs: As discussed above this is straightforward in the case of large diameter SWNTs, but for species of smaller diameter such as HiPCO-SWNTs there are severe steric barriers to the incorporation of a molecule such as S_8. The suggested mechanism for encapsulation is given below in which we conjecture that the sulfur species that enters the SWNTs is S_2 ($^3\Sigma_g^-$); given a van der Waals radius for sulfur of 0.185 nm, the S_2 molecule fits easily inside the HiPCO-SWNTs (Scheme 1).

Scheme 1. Proposed Mechanism for Encapsulation and Removal of Sulfur in SWNTs via Intermediacy of S_2 ($^3\Sigma_g^-$)

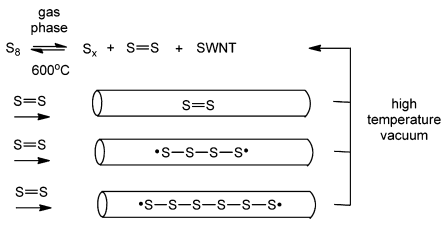

Once inside the SWNTs the S_2 molecules would be expected to polymerize to diradicals particularly after cooling to room temperature. The encapsulation experiments are run at 600 °C in a static vacuum, and we note that thermodynamic analysis indicates that S_2 comprises ∼5% of the vapor above sulfur at 500 °C under a total pressure of 0.2 MPa, and thus it will be possible to rapidly fill the SWNTs with S_2.[40−42] High-level calculations

DOI: 10.1021/jacs.5b10598
J. Am. Chem. Soc. 2016, 138, 40−43

confirm that cis- and trans-isomers of S_4 are considerably more stable than 2 S_2 ($^3\Sigma_g^-$),[43] and so the dimerization and subsequent polymerization reactions should occur spontaneously under the reaction conditions.

Based on this mechanism, the removal of sulfur at elevated temperatures would involve a simple reversal of the forward steps shown in the diagram. XPS measurements show 8 atomic percent internal sulfur after encapsulation experiments on HiPCO-SWNTs, which is reduced to 2% after treatment at 450 °C (Figure S6).

In summary, we suggest that gas-phase sulfur is incorporated into the interior of small diameter SWNTs by the initial encapsulation of S_2 molecules, where they undergo polymerization to give long chain S_x diradicals. The polymeric sulfur chain strongly interacts with the sidewalls of the HiPCO-SWNTs resulting in a shift of the near-IR interband electronic transitions to lower energy by more than 10%. In addition, there are large changes in the Raman spectra with the high frequency bands ($\nu >$ 1200 cm^{-1}) decreased in intensity and the appearance of new, very strong bands at 319, 395, and 715 cm^{-1} which originate from the encapsulated sulfur species as a result of strong electron−phonon coupling between the SWNT excitons and the sulfur−sulfur vibrations.

■ ASSOCIATED CONTENT

Supporting Information

The Supporting Information is available free of charge on the ACS Publications website at DOI: 10.1021/jacs.5b10598.

Figures and computation results (PDF)

■ AUTHOR INFORMATION

Corresponding Author

*haddon@ucr.edu

Notes

The authors declare no competing financial interest.

■ ACKNOWLEDGMENTS

This material is based upon work supported by Vice Chancellor for Research and Economic Development, University of California, Riverside.

■ REFERENCES

(1) Guo, J.; Xu, Y.; Wang, C. *Nano Lett.* **2011**, *11*, 4288.
(2) Zheng, G.; Yang, Y.; Cha, J. J.; Hong, S. S.; Cui, Y. *Nano Lett.* **2011**, *11*, 4462.
(3) Dörfler, S.; Hagen, H.; Althues, H.; Tübke, J.; Kaskel, S. *Chem. Commun.* **2012**, *48*, 4097.
(4) Zhou, G.; Wang, D.; Li, F.; Hou, P.; Yin, L.; Liu, C.; Lu, G.; Gentle, I. R.; Cheng, H. *Energy Environ. Sci.* **2012**, *5*, 8901.
(5) Fujimori, T.; Morelos-Gómez, A.; Zhu, Z.; Muramatsu, H.; Futamura, R.; Urita, K.; Terrones, M.; Hayashi, T.; Endo, M.; Hong, S. Y.; Choi, Y. C.; Tomanek, D.; Kaneko, K. *Nat. Commun.* **2013**, *4*, 3162.
(6) Yang, C.; Yin, Y.; Guo, Y.; Wan, L. *J. Am. Chem. Soc.* **2015**, *137*, 2215.
(7) Loiseau, A.; Pascard, H. *Chem. Phys. Lett.* **1996**, *256*, 246−252.
(8) Demoncy, N.; Stephan, O.; Brun, N.; Colliex, C.; Loiseau, A.; Pascard, H. *Synth. Met.* **1999**, *103*, 2380.
(9) Hamon, M. A.; Itkis, M. E.; Niyogi, S.; Alvaraez, T.; Kuper, C.; Menon, M.; Haddon, R. C. *J. Am. Chem. Soc.* **2001**, *123*, 11292.
(10) Wang, F.; Itkis, M. E.; Haddon, R. C. *Nano Lett.* **2010**, *10*, 937.
(11) Wang, F.; Itkis, M. E.; Bekyarova, E.; Haddon, R. C. *Nat. Photonics* **2013**, *7*, 459.
(12) Tian, X.; Moser, M. L.; Pekker, A.; Sarkar, S.; Ramirez, J.; Bekyarova, E.; Itkis, M. E.; Haddon, R. C. *Nano Lett.* **2014**, *14*, 3930.
(13) Dresselhaus, M. S.; Dresselhaus, G.; Eklund, P. C. *Science of Fullerenes and Carbon Nanotubes*; Academic Press: San Diego, CA, 1996.
(14) Bachilo, S. M.; Strano, M. S.; Kittrell, C.; Hauge, R. H.; Smalley, R. E.; Weisman, R. B. *Science* **2002**, *298*, 2361.
(15) O'Connell, M. J.; Bachilo, S. M.; Huffman, C. B.; Moore, V. C.; Strano, M. S.; Haroz, E. H.; Rialon, K. L.; Boul, P. J.; Noon, W. H.; Kittrell, C.; Ma, J.; Hauge, R. H.; Weisman, R. B.; Smalley, R. E. *Science* **2002**, *297*, 593.
(16) Ostojic, G. N.; Zaric, S.; Kono, J.; Strano, M. S.; Moore, V. C.; Hauge, R. H.; Smalley, R. E. *Phys. Rev. Lett.* **2004**, *92*, 117402.
(17) Klan, P.; Wirz, J. *Photochemistry of Organic Compounds: From Concepts to Practice*; Wiley: Chichester, U.K., 2009.
(18) Blase, X.; Benedict, L. X.; Shirley, E. L.; Louie, S. G. *Phys. Rev. Lett.* **1994**, *72*, 1878.
(19) Wu, J.; Walukiewicz; Shan, W.; Bourret-Courchesne, E.; Ager, J. W., III; Yu, K. M.; Haller, E. E.; Kissell, K.; Bachilo, S. M.; Weisman, R. B.; Smalley, R. E. *Phys. Rev. Lett.* **2004**, *93*, 017404.
(20) Charlier, J.-C.; Lambin, P.; Ebbesen, T. W. *Phys. Rev. B: Condens. Matter Mater. Phys.* **1996**, *54*, R8377−R8380.
(21) Haddon, R. C.; Scuseria, G. E.; Smalley, R. E. *Chem. Phys. Lett.* **1997**, *272*, 38.
(22) Haddon, R. C. *Science* **1993**, *261*, 1545.
(23) Arnold, K.; Lebedkin, S.; Kiowski, O.; Hennrich, F.; Kappes, M. M. *Nano Lett.* **2004**, *4*, 2349.
(24) Yang, L.; Anantram, M. P.; Han, J.; Lu, J. P. *Phys. Rev. B: Condens. Matter Mater. Phys.* **1999**, *60*, 13874.
(25) Yang, L.; Han, J. *Phys. Rev. Lett.* **2000**, *85*, 154.
(26) Rao, A. M.; Richter, E.; Bandow, S.; Chase, B.; Eklund, P. C.; Williams, K. A.; Fang, S.; Subbaswamy, K. R.; Menon, M.; Thess, A.; Smalley, R. E.; Dresselhaus, G.; Dresselhaus, M. *Science* **1997**, *275*, 187.
(27) Kavan, L.; Rapta, P.; Dunsch, L.; Bronikowski, M. J.; Willis, P.; Smalley, R. E. *J. Phys. Chem. B* **2001**, *105*, 10764.
(28) Rao, A. M.; Chen, J.; Richter, E.; Eklund, P. C.; Haddon, R. C.; Venkateswaran, U. D.; Kwon, Y.-K.; Tomanek, D. *Phys. Rev. Lett.* **2001**, *86*, 3895.
(29) Corio, P.; Santos, P. S.; Brar, V. W.; Samsonidze, G. G.; Chou, S. G.; Dresselhaus, M. S. *Chem. Phys. Lett.* **2003**, *370*, 675.
(30) Cronin, S. B.; Barnett, R.; Tinkham, M.; Chou, S. G.; Rabin, O.; Dresselhaus, M. S.; Swan, A. K.; Ünlü, M. S.; Goldberg, B. B. *Appl. Phys. Lett.* **2004**, *84*, 2052.
(31) Rafailov, P. M.; Maultzsch, J.; Thomsen, C.; Kataura, H. *Phys. Rev. B: Condens. Matter Mater. Phys.* **2005**, *72*, 045411.
(32) Das, A.; Sood, A. K.; Govindaraj, A.; Saitta, A. M.; Lazzeri, M.; Mauri, F.; Rao, C. R. *Phys. Rev. Lett.* **2007**, *99*, 136803.
(33) Bushmaker, A. W.; Deshpande, V. V.; Hsieh, S.; Bockrath, M.; Cronin, S. B. *Phys. Rev. Lett.* **2009**, *103*, 067401.
(34) Saito, R.; Dresselhaus, G.; Dresselhaus, M. S. *Physical Properties of Carbon Nanotubes*; Imperial College Press: Singapore, 1998.
(35) Jorio, A.; Souza Filho, A. G.; Dresselhaus, G.; Dresselhaus, M. S.; Saito, R.; Hafner, J. H.; Lieber, C. M.; Matinaga, F. M.; Dantas, M. S. S.; Pimenta, M. A. *Phys. Rev. B: Condens. Matter Mater. Phys.* **2001**, *63*, 245416.
(36) Fantini, C.; Jorio, A.; Souza, M.; Strano, M. S.; Dresselhaus, M. S.; Pimenta, M. A. *Phys. Rev. Lett.* **2004**, *93*, 147406.
(37) Saito, R.; Hofmann, M.; Dresselhaus, G.; Jorio, A.; Dresselhaus, M. S. *Adv. Phys.* **2011**, *60*, 413.
(38) Barletta, R. E.; Claassen, H. H.; McBeth, R. L. *J. Chem. Phys.* **1971**, *55*, 5409.
(39) Eckert, B.; Steudel, R. *Top. Curr. Chem.* **2003**, *231*, 31.
(40) Rau, h.; Kutty, T. R. N.; Guedes De Carvalho, J. R. F. *J. Chem. Thermodyn.* **1973**, *5*, 291.
(41) Rau, H.; Kutty, T. R. N.; Guedes De Carvalho, J. R. F. *J. Chem. Thermodyn.* **1973**, *5*, 833.
(42) Steudel, R.; Steudel, Y.; Wong, M. W. *Top. Curr. Chem.* **2003**, *230*, 117.
(43) Wong, M. W.; Steudel, R. *Chem. Phys. Lett.* **2003**, *379*, 162.

DOI: 10.1021/jacs.5b10598
J. Am. Chem. Soc. 2016, 138, 40−43

Supporting Information

Giant Raman Response to the Encapsulation of Sulfur in Narrow Diameter Single-Walled Carbon Nanotubes

Guanghui Li,[1,3] Chengyin Fu,[1] M. Belén Oviedo,[1] Mingguang Chen,[1,3] Xiaojuan Tian,[1,3] Elena Bekyarova,[2,3] Mikhail E. Itkis,[2,3] Bryan M. Wong,[1]* Juchen Guo,[1]* and Robert C. Haddon[1-3]*

[1]Department of Chemical Engineering, University of California, Riverside, California 92521, United States

[2]Department of Chemistry, University of California, Riverside, California 92521, United States

[3]Center for Nanoscale Science and Engineering, University of California, Riverside, California 92521, United States

Raman and UV-Vis-NIR Spectroscopy

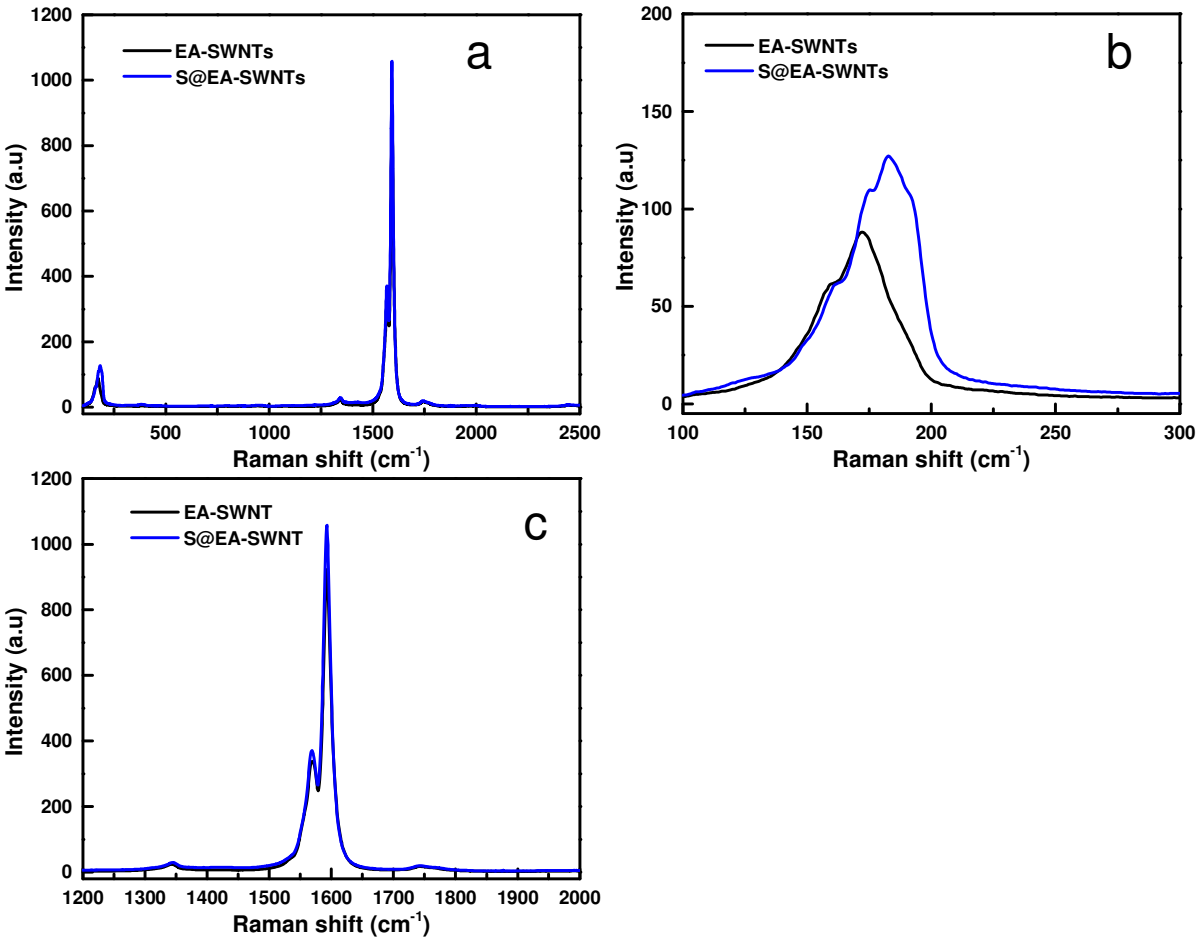

Figure S1. Raman spectra of EA-SWNTs and S@EA-SWNTs: (a) full spectrum, (b) RBM region, (c) G-peak region (laser excitation wavelength: 532 nm).

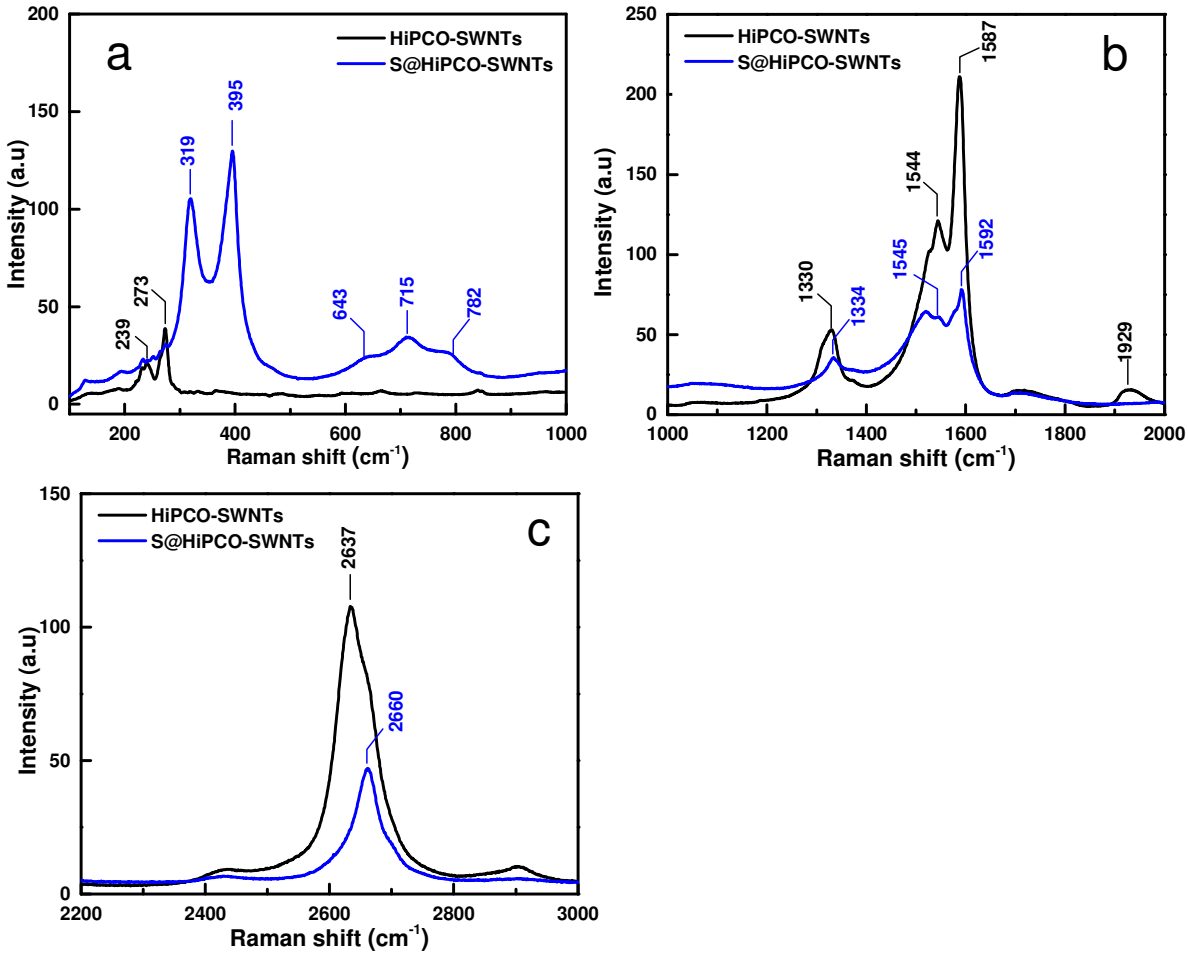

Figure S2. Raman spectra of HiPCO-SWNTs and S@HiPCO-SWNTs films: (a) RBM and IFM region, (b) G-peak region, (c) 2D-peak region (laser excitation wavelength: 532 nm).

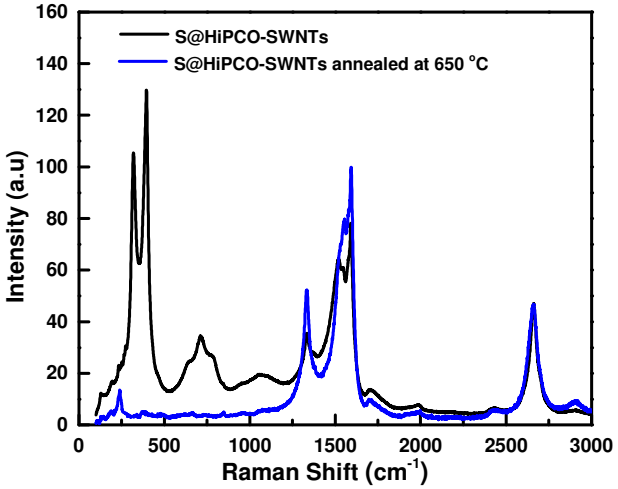

Figure S3. Raman spectra of S@HiPCO-SWNTs and S@HiPCO-SWNTs annealed at 650 °C in Ar atmosphere.

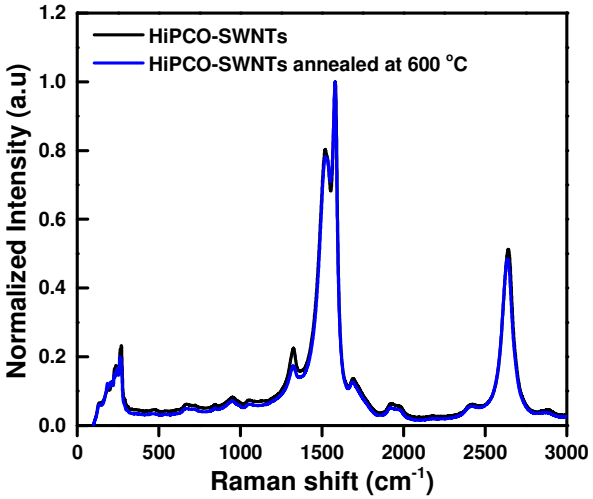

Figure S4. Raman spectra of HiPCO-SWNTs and HiPCO-SWNTs annealed at 600 °C in Ar atmosphere.

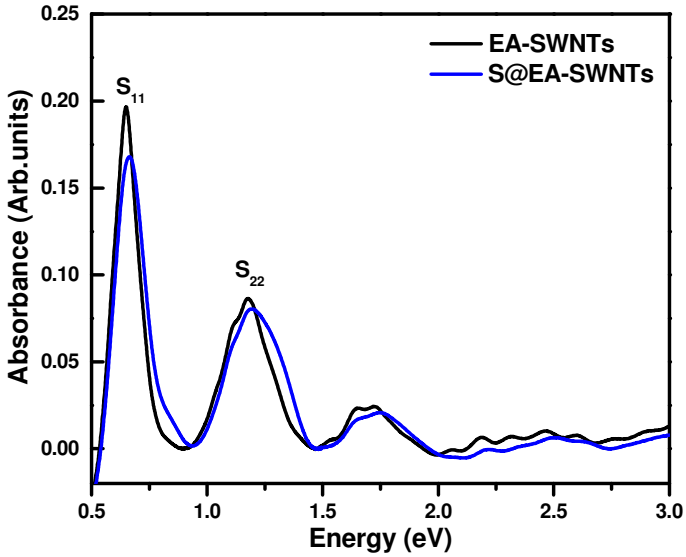

Figure S5. Base-line subtracted NIR/VIS absorption spectra of EA-SWNTs and S@EA-SWNTs films.

Table S1. Peak assignments for the NIR/VIS spectra of HiPCO-SWNTs and S@HiPCO-SWNTs films.

Peaks		SWNTs (eV)	S@ SWNTs (eV)	Shift (eV)
S11	#1	0.948	0.826	0.122
	#2	1.046	0.907	0.139
S22	#3	1.504	1.260	0.244
	#4	1.650	1.349	0.301
M11	#5	1.856	1.481	0.375
	#6	2.042	1.625	0.417
	#7	2.181	1.750	0.431
	#8	2.404	1.858	0.546
	#9	2.679	1.991	0.688

Table S2: Raman spectral peaks for ^{32}S@HiPCO and ^{34}S@HiPCO (cm^{-1}).

^{32}S@HiPCO-SWNTs (cm^{-1})	^{34}S@HiPCO-SWNTs (cm^{-1})	$\nu_1(^{34}S)/\nu_1(^{32}S)$	Theoretical $(32/34)^{1/2}$
319	311	0.975	
395	385	0.975	
643	625	0.972	0.970
715	694	0.970	
782	769	0.983	

XPS analysis

The X-ray photoelectron spectroscopy (XPS) was performed using a Kratos AXIS ULTRADLD XPS system equipped with an Al Kα monochromated X-ray source. The vacuum pressure was kept below 3×10^{-9} torr and a charge neutralizer was applied during the data acquisition. The survey spectra were recorded using 0.5 eV step size, 100 ms dwell time, and 80 pass energy. The high-resolution spectra were recorded with 0.05 eV step size, 200 ms dwell time, and 20 pass energy. For the measurements, 8 nm thin films were transferred on glass substrates.

The survey spectrum of S@HiPCO SWNTs clearly showed the presence of sulfur, whereas no sulfur peaks were detected in the survey spectra of S@HiPCO SWNTs annealed at 450 ^{o}C in vacuum. Both spectra show a strong C1s peak, and the additional peaks - O1s, Si2s, and Si2p - are assigned to the glass substrate; XPS spectra of powdered materials (not shown) showed traces of oxygen content. The high resolution C1s spectra of S@HiPCO SWNTs and S@HiPCO SWNTs annealed at 450 ^{o}C (Figure S6c), show that the SWNTs are largely preserved after the annealing process, while the S2p spectra (Figure 6Sd) illustrates that after annealing the sulfur content is significantly reduced.

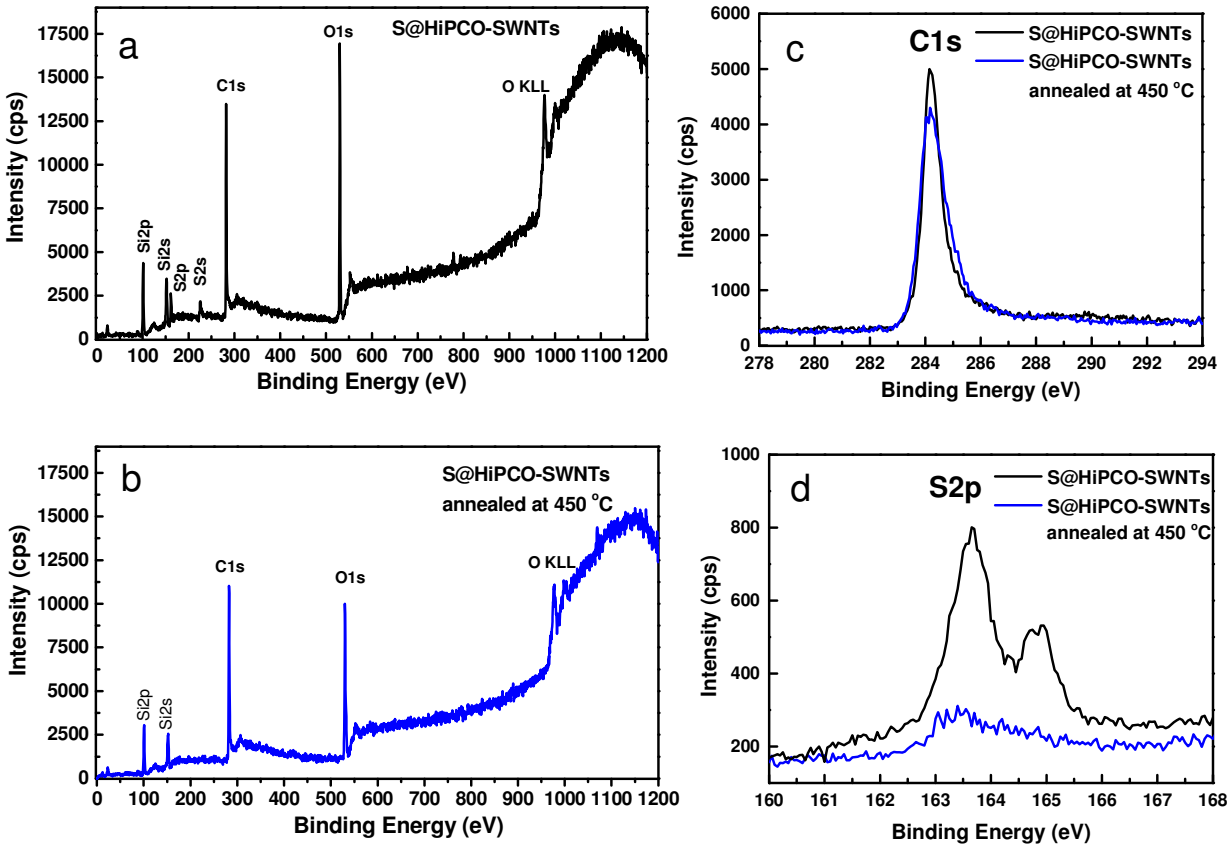

Figure S6. (a) Survey spectrum of S@HiPCO SWNTs. (b) Survey spectrum of S@HiPCO-SWNT annealed at 450 °C in vacuum. (c) C1s spectra of S@HiPCO SWNTs and S@HiPCO SWNTs annealed at 450 °C in vacuum. (d) S2p spectra of S@HiPCO SWNTs and S@HiPCO SWNTs annealed at 450 °C in vacuum.

Computational Details

All geometry optimizations were carried out for a system composed of a (11, 11) (Figure S7) and a (7, 7) (Figure S8) SWCNT filled with a sulfur chain in three different configurations: (a) linear, (b) zigzag, and (c) helix. Geometry optimizations were carried out with the VASP code with a plane-wave basis and periodic boundary conditions,[1,2] where the projector augmented wave (PAW) method was used to numerically represent the electronic wave functions.[3, 4] We used the nonlocal optB86b-vdW exchange-correlation functional which explicitly calculates van der Waals effects (via nonlocal double real-space integrals of the electron density) to account for the dispersion interactions between the SWCNT and the sulfur chain.[5] A 4×1×1 mesh of k points was implemented for the Brillouin zone integration,[6] and a 402 eV energy cutoff was

used for the electronic wavefunctions. A vacuum region of ~30 Å was used in the y and z-directions, and periodic boundary conditions were applied in all three dimensions.

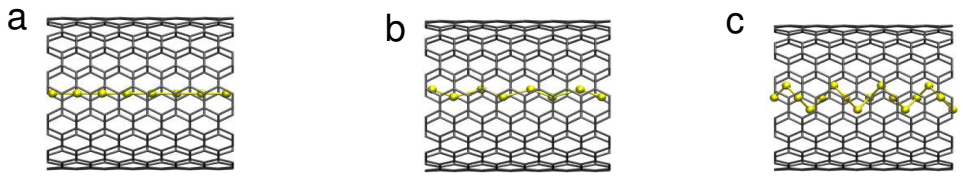

Figure S7. Optimized geometries of (a) linear, (b) zigzag, and (c) helix configuration for the sulfur chain inside a (11,11) SWNT.

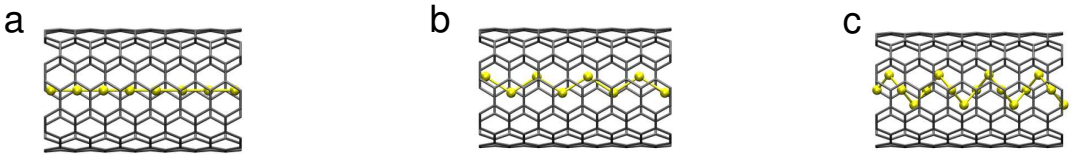

Figure S8. Optimized geometries of (a) linear, (b) zigzag, and (c) helix configuration for the sulfur chain inside a (7,7) SWNT.

Tables S2 and S3 give the total electronic energy of S@(7,7) SWNT and S@(11,11) SWNT respectively, for different geometrical configurations of the sulfur chain. In order to determine the most energetically favorable molecular configuration inside the SWNT we calculated the cohesive energy, defined as follows:

$E_{coh} = (E_{total} - E_{CNT} - n \cdot E_S) / n$

Where E_{total} is the total electronic energy of the entire system, E_{CNT} is the electronic energy of the SWNT without the sulfur chain, E_S is the electronic energy of a single sulfur atom in vacuum, and n is the number of sulfur atoms inside the SWNT. The value of E_{coh} determines the stability of the molecular configuration of the sulfur chain inside the SWNT. From the values of the cohesive energy we can determine that the most stable molecular configuration of the sulfur chain is the helix shape for both SWNTs.

Table S3: Total electronic and cohesive energies for a linear, zigzag, and helix configuration of the sulfur chain inside a (7,7) SWNT. ECNT = −1566.269 eV and ES = −1.611 eV.

Chain configuration	Total Energy (eV)	Cohesive Energy (eV)
Linear	−1582.099	−0.367
Zigzag	−1582.726	−0.445
Helix	−1607.425	−0.961

Table S4: Total electronic and cohesive energies for a linear, zigzag and helix configuration of the sulfur chain inside a (11,11) SWNT. ECNT = −2476.645 eV and ES = −1.611 eV.

Chain configuration	Total Energy (eV)	Cohesive Energy (eV)
Linear	−2489.873	−0.042
Zigzag	−2490.389	−0.107
Helix	−2513.169	−0.672

References

(1) G. Kresse and J. Furthmüller. Comput. Mater. Sci. 1996, 6, 15-50.

(2) G. Kresse and J. Furthmüller. Phys. Rev. B. 1996, 54, 11169-11186.

(3) P. E. Blöchl. Phys. Rev. B. 1994, 50, 17953-17979.

(4) G. Kresse and D. Joubert. Phys. Rev. B. 1999, 59, 1758-1775.

(5) J. Klimeš, D. R. Bowler, A. Michaelides. Phys. Rev. B. 2011, 83, 195131.

(6) H. J. Monkhorst and J. D. Pack. Phys. Rev. B. 1976, 13, 5188-5192.